

Optimal Interplanetary Rendezvous Combining Electric Sail and High Thrust Propulsion System

Alessandro A. Quarta , Giovanni Mengali *

Dipartimento di Ingegneria Aerospaziale, University of Pisa, I-56122 Pisa, Italy

and

Pekka Janhunen

Finnish Meteorological Institute, FIN-00101 Helsinki, Finland

Abstract

The aim of this paper is to study, from a mission analysis point of view, the performance of an hybrid propulsion concept for a two-dimensional transfer towards a planet of the Solar System. The propulsion system is obtained by combining a chemical thruster, used for the phases of Earth escape and target capture, with an electric sail, which provides a continuous thrust during the heliocentric transfer. Two possible mission scenarios are investigated: in the first case the sailcraft reaches the target with zero hyperbolic excess velocity (thus performing a classical rendezvous mission). In the second mission scenario, a given final hyperbolic excess speed is tolerated in order to decrease the total flight time. The amount of final hyperbolic excess speed is used as a simulation parameter for a tradeoff study in which the minimum flight time is related to the total velocity variation required by the chemical thruster to accomplish the mission.

Key words: Electric Sail, Trajectory Optimization, Hybrid propulsion system

Nomenclature

a	=	semimajor axis of osculating orbit
a_{\oplus}	=	sailcraft characteristic acceleration
b_1, b_2, b_3	=	fitting coefficients (see Eq. (23))
C_3	=	escape orbit characteristic energy
e	=	eccentricity of osculating orbit
h_c	=	circular parking orbit altitude
h_p	=	periapse altitude of capture orbit
H	=	Hamiltonian
H'	=	reduced Hamiltonian
I_{sp}	=	specific impulse
J	=	performance index
m	=	mass
r	=	Sun-sailcraft distance ($r_{\oplus} \triangleq 1 \text{ AU}$)
r_p	=	target planet heliocentric orbit radius
R_p	=	target planet mean radius
R_{\oplus}	=	Earth's mean radius
t	=	time
u	=	radial velocity component
v	=	circumferential velocity component
V_{∞}	=	hyperbolic excess velocity w.r.t. the target planet
α	=	sail cone angle

* Corresponding author.

Email addresses: a.quarta@ing.unipi.it (Alessandro A. Quarta),
g.mengali@ing.unipi.it (Giovanni Mengali), pekka.janhunen@fmi.fi
(Pekka Janhunen).

α_λ	=	primer vector cone angle
ΔV	=	impulsive velocity variation
θ	=	polar angle
$\boldsymbol{\lambda}$	=	primer vector ($\lambda \triangleq \ \boldsymbol{\lambda}\ $)
λ_i	=	adjoint variables associated with the i -th state variable
μ	=	gravitational parameter
σ	=	mass fraction
τ	=	switching parameter

Subscripts

0	=	initial
C	=	chemical
cap	=	capture
E	=	hybrid
esc	=	escape
f	=	final
H	=	Hohmann
max	=	maximum
pay	=	payload
prop	=	propellant
sail	=	electric sail
tot	=	total
\odot	=	Sun

Superscripts

\cdot	=	time derivative
\star	=	critical
τ	=	transpose
$\hat{}$	=	unit vector

1 Introduction

An interplanetary mission transfer usually requires large changes in orbital energy. For conventional (chemical) propulsion systems the high necessary ΔV corresponds to a considerable propellant mass required to accomplish the mission. Gravity assisted maneuvers can in principle be incorporated into the trajectory design to reduce the spacecraft launch mass, but such a strategy substantially increases both the mission complexity and the flight time [1,2]. A possible alternative to reduce the total propellant mass is obtained by combining a chemical thruster with a low-thrust propulsion system, whose employment is especially useful during the long phase of heliocentric transfer [3,4,5,6,7,8]. In this context, an interesting option is offered by an electric sail. The latter is an innovative propulsion concept that, similar to a more conventional solar sail [9,10,11,12], allows a spacecraft to deliver a payload to some high-energy orbit without the need for reaction mass. The spacecraft is spun around the symmetry axis and the rotational motion is used to deploy approximately one hundred long conducting tethers held at a high positive or negative potential [13,14] through an electron gun, whose electron beam is shot roughly along the spin axis. The resulting static electric field of the tethers perturbs the trajectories of the incident solar wind protons, thus producing a momentum transfer from the solar wind plasma stream to the tethers [15]. For an in depth discussion of the electric sail arrangement and of his main characteristics, the reader is referred to Refs. [16,17,18,19,20]

and to the companion paper [21]. Because an electric sail cannot operate inside the planetary magnetosphere, an interplanetary mission strategy is likely to use additional and high-thrust propulsion systems for the escape and capture phases. This may be referred to as a hybrid configuration [22,23], and is actually the starting point of our analysis. More precisely, the aim of this paper is to study, from a mission design point of view, the performance of such a hybrid propulsion concept for a two-dimensional transfer towards a planet of the Solar System. We show that this solution may represent a viable option for mission design.

2 Mission Design

The heliocentric equations of motion for an electric sailcraft in an heliocentric polar inertial frame $\mathcal{T}_\odot(r, \theta)$ are

$$\dot{r} = u \tag{1}$$

$$\dot{\theta} = \frac{v}{r} \tag{2}$$

$$\dot{u} = \frac{v^2}{r} - \frac{\mu_\odot}{r^2} + a_\oplus \tau \cos \alpha \left(\frac{r_\oplus}{r} \right)^{7/6} \tag{3}$$

$$\dot{v} = -\frac{uv}{r} + a_\oplus \tau \sin \alpha \left(\frac{r_\oplus}{r} \right)^{7/6} \tag{4}$$

where μ_\odot is the Sun's gravitational parameter, r is the Sun-sailcraft distance, θ is the polar angle of the sailcraft (measured anticlockwise from a fixed reference direction), u and v are the radial and circumferential component of velocity, a_\oplus is the sail characteristic acceleration (i.e., the maximum propelling acceleration at $r = r_\oplus \triangleq 1$ AU).

In Eqs. (3)-(4) terms $\tau = (0, 1)$ and $\alpha \in [-\alpha_{\max}, \alpha_{\max}]$, with $\alpha_{\max} \triangleq \max(\alpha) < \pi/2$, are the control variables. The switching parameter τ models the electric sail on/off condition and is

introduced to account for coasting arcs in the spacecraft trajectory, while the sail cone angle α is the angle between the Sun-sailcraft line and the sailcraft thrust direction, see Fig. 1.

At the initial time instant $t_0 \triangleq 0$ the sailcraft is on a circular orbit around the Sun with radius $r = r_{\oplus}$. The four initial conditions for the state variables are:

$$r(t_0) = r_{\oplus} \quad , \quad \theta(t_0) \equiv u(t_0) = 0 \quad , \quad v(t_0) = \sqrt{\mu_{\odot}/r_{\oplus}} \quad (5)$$

The problem is to find the minimum flight time t_f necessary to perform a flyby with a planet in the Solar System. For the sake of mathematical tractability all of the planets orbits are approximated as circular (with radius r_p) and coplanar to the initial orbit. From a mathematical viewpoint, for a given pair a_{\oplus}, r_p the optimal trajectory is the one that maximizes the performance index $J = -t_f$.

In this study the final hyperbolic excess velocity V_{∞} is given. Because the target body orbit is circular, one has

$$V_{\infty}^2 = \left[v(t_f) - \sqrt{\mu_{\odot}/r_p} \right]^2 + u(t_f)^2 \quad (6)$$

In particular, $V_{\infty} = 0$ corresponds to a rendezvous trajectory, and Eq. (6) provides two scalar conditions, viz.

$$u(t_f) = 0 \quad , \quad v(t_f) = \sqrt{\mu_{\odot}/r_p} \quad (7)$$

Note that V_{∞} coincides with the velocity variation necessary to circularize the orbit at the final time t_f by means of a single impulsive maneuver. Accordingly, the problem may be thought of as being equivalent to the minimum flight time for a planetary rendezvous mission of a spacecraft with a hybrid propulsion system. The latter is composed by an electric sail plus a chemical propeller, which is capable of providing the final value of V_{∞} necessary to complete the rendezvous mission.

The minimum time problem has been solved through an indirect approach, by maximizing the

Hamiltonian:

$$H = \lambda_r u + \lambda_\theta \frac{v}{r} + \lambda_u \left(\frac{v^2}{r} - \frac{\mu_\odot}{r^2} \right) - \lambda_v \frac{u v}{r} + H' \quad (8)$$

where λ_r , λ_θ , λ_u and λ_v are the adjoint variables associated with the state variables r , θ , u , and v , respectively, and H' coincides with that portion of the Hamiltonian that explicitly depends on the controls (τ, α) , that is:

$$H' \triangleq a_\oplus \tau (\lambda_u \cos \alpha + \lambda_v \sin \alpha) \left(\frac{r_\oplus}{r} \right)^{7/6} \quad (9)$$

The time derivatives of the adjoint variables are provided by the Euler-Lagrange equations [16,24]:

$$\dot{\lambda}_r = \frac{\lambda_\theta v}{r^2} + \lambda_u \left(\frac{v^2}{r^2} - \frac{2\mu_\odot}{r^3} \right) - \lambda_v \frac{u v}{r^2} + \frac{7 H'}{6 r} \quad (10)$$

$$\dot{\lambda}_\theta = 0 \quad (11)$$

$$\dot{\lambda}_u = -\lambda_r + \lambda_v \frac{v}{r} \quad (12)$$

$$\dot{\lambda}_v = -\frac{\lambda_\theta}{r} - 2 \frac{\lambda_u v}{r} + \frac{\lambda_v u}{r} \quad (13)$$

2.1 Optimal Control Law

From Pontryagin's maximum principle, an optimal control law is found by maximizing, at all times, the reduced Hamiltonian function H' , see Eq. (9). In analogy with Lawden [25], it is useful to introduce the primer vector $\boldsymbol{\lambda}$, defined as

$$\boldsymbol{\lambda} \triangleq \lambda [\cos \alpha_\lambda, \sin \alpha_\lambda]^T \quad (14)$$

where

$$\lambda \triangleq \sqrt{\lambda_u^2 + \lambda_v^2} \quad (15)$$

and $\alpha_\lambda \in [-\pi, \pi]$ is the primer vector cone angle:

$$\cos \alpha_\lambda \triangleq \lambda_u/\lambda \quad , \quad \sin \alpha_\lambda \triangleq \lambda_v/\lambda \quad (16)$$

The propelling acceleration unit vector $\hat{\mathbf{a}}$ can be expressed in a rotating reference frame as $\hat{\mathbf{a}} \triangleq [\cos \alpha, \sin \alpha]^T$. Accordingly, H' can be rewritten in compact form as

$$H' = a_\oplus \tau \lambda \left(\hat{\boldsymbol{\lambda}} \cdot \hat{\mathbf{a}} \right) \left(\frac{r_\oplus}{r} \right)^{7/6} \quad (17)$$

where $\hat{\boldsymbol{\lambda}} \triangleq \boldsymbol{\lambda}/\lambda$ is the primer unit vector. Equation (17) states that the optimal cone angle α is found by maximizing $\hat{\mathbf{a}}$ in the direction of $\hat{\boldsymbol{\lambda}}$. Recalling that there exists an upper admissible cone angle $\alpha_{\max} < \pi/2$, the two possible cases are summarized in Fig. 2. If $|\alpha_\lambda| \leq \alpha_{\max}$ (see Fig. 2(a)), H' is maximized when $\hat{\mathbf{a}} = \hat{\boldsymbol{\lambda}}$. This situation corresponds to the optimal control law for an electric propulsion system [7,26,27]. Otherwise, that is, if $|\alpha_\lambda| > \alpha_{\max}$ (see Fig. 2(b)), $\hat{\mathbf{a}}$ must lie on the boundary of the thruster operating cone in order to minimize the difference $|\alpha_\lambda - \alpha|$. By combining the two above cases, the optimal steering law is

$$\alpha = \begin{cases} \alpha_\lambda & \text{if } |\alpha_\lambda| \leq \alpha_{\max} \\ \text{sign}(\alpha_\lambda) \alpha_{\max} & \text{if } |\alpha_\lambda| > \alpha_{\max} \end{cases} \quad (18)$$

where $\text{sign}(\cdot)$ is the signum function. Finally, the optimal switching law is found observing that H' depends linearly on τ . As a result, a bang-bang control [28] is optimal:

$$\tau = \begin{cases} 1 & \text{if } \hat{\boldsymbol{\lambda}} \cdot \hat{\mathbf{a}} \geq 0 \\ 0 & \text{if } \hat{\boldsymbol{\lambda}} \cdot \hat{\mathbf{a}} < 0 \end{cases} \quad (19)$$

In particular, note that $\tau = 0$ when $\alpha_\lambda \geq \alpha_{\max} + \pi/2$. Assuming $\alpha_{\max} = 35 \text{ deg}$ [13,15,18], the optimal control law for α is shown in Fig. 3 as a function of α_λ .

2.2 Boundary Conditions

The four equations of motion (1)–(4) and the four Euler-Lagrange equations (10)–(13) must be completed by eight suitable boundary conditions. Four initial conditions are provided by Eq. (5). A fifth condition is obtained by imposing that the final spacecraft distance coincides with the target orbit radius, that is

$$r(t_f) = r_p \quad (20)$$

Moreover, assuming that the final spacecraft angular position is left free, yields

$$\lambda_\theta(t_f) = 0 \quad (21)$$

Recalling Eq. (11), Eq. (21) implies that $\lambda_\theta = \text{constant} = 0$. Equation (21) allows one to find the minimum transfer times independent of the ephemeris constraints on the angular positions of the celestial bodies.

The two remaining boundary conditions take different values according to whether V_∞ is zero or not. When $V_\infty \neq 0$, a boundary condition is given by Eq. (6), while the other is [24]

$$\lambda_u(t_f) \left(v(t_f) - \sqrt{\mu_\odot/r_p} \right) = \lambda_v(t_f) u(t_f) \quad (22)$$

If, instead, $V_\infty = 0$, the two missing boundary conditions are given by Eq. (7). Finally, for both cases $V_\infty = 0$ and $V_\infty \neq 0$ the minimum flight time is found by enforcing the transversality condition $H(t_f) = 1$.

3 Numerical Simulations

The previous optimal control law has been used to find the minimum time trajectories for missions towards planets in the Solar System, under the simplified assumption of circular planetary orbits. Each transfer mission has been investigated in a parametric way for different values of characteristic acceleration and hyperbolic excess speed with respect to the target planet. The obtained results have been arranged in graphs in which the hyperbolic excess speed V_∞ and the flight time t_f are made dimensionless by dividing their values for the velocity variation ΔV_H and mission time t_H corresponding to an Hohmann heliocentric transfer. These reference values are summarized in Table 1. In all of the simulations, the differential equations have been integrated in double precision using a variable order Adams-Bashforth-Moulton solver with absolute and relative errors of 10^{-12} . The final boundary constraints were set to 100 km for the position error and 0.05 m/s for the velocity error. These tolerance limits are consistent for purposes of preliminary mission analysis.

3.1 Missions Towards Inner Planets

Earth-Mercury trajectories have been studied by varying the characteristic acceleration in the range $a_\oplus \in [1, 2] \text{ mm/s}^2$ and the hyperbolic excess speed in the range $V_\infty \in [0, 0.5] \Delta V_H$ (from Table 1, $0.5 \Delta V_H$ corresponds to about 8.57 km/s). Note that the results based on a circular heliocentric orbit of Mercury are not accurate. In fact Mercury has the largest orbital inclination (about 7 deg) of all planets. A maneuver involving an inclination variation of 7 deg costs at least 3.6 km/s in terms of ΔV , and even more so for an electric-sail mission in which the inclination change cannot be impulsive. The simulation results are shown in Fig. 4. Note that in Fig. 4(b) the parameter $t_{\text{on}} \leq t_f$, that is, the time in which the propulsion system is on, has been displayed as a function of V_∞ and a_\oplus . A rendezvous mission towards Mercury

with an electric sail of mean performance ($a_{\oplus} = 1 \text{ mm/s}^2$) requires a minimum flight time of 9 months. The propulsion system is on for about the 80% of the total mission time. Note that t_{on} is not very sensitive to variations in V_{∞} , while it is much more affected by the sail characteristic acceleration. Although an increase in V_{∞} corresponds to a flight time decrease, however such a reduction is not marked. For example, assuming $V_{\infty} = 0.5 \Delta V_H \simeq 8.57 \text{ km/s}$, the flight time is 7.17 months, with a reduction of 20% only with respect to the rendezvous case ($V_{\infty} = 0$).

The results for Earth-Venus missions, calculated with $a_{\oplus} \in [0.5, 2] \text{ mm/s}^2$ and $V_{\infty} \in [0, 1] \Delta V_H \simeq [0, 5.2] \text{ km/s}$, are summarized in Fig. 5. In this case, due to the small eccentricity of Venus' orbit ($e \simeq 6.77 \times 10^{-3}$), the results for circular orbits are much more representative of a realistic transfer. A rendezvous mission with a sailcraft having $a_{\oplus} = 1 \text{ mm/s}^2$ requires 6.8 months only. Note that if one halves the characteristic acceleration (for example, by doubling the spacecraft total mass) the flight time increase does not exceed the 22%. Accordingly, an increase in the hyperbolic excess speed at arrival does not provide a substantial advantage in terms of flight time.

The results for Earth-Mars missions, calculated with $a_{\oplus} \in [0.5, 2] \text{ mm/s}^2$ and $V_{\infty} \in [0, 1] \Delta V_H \simeq [0, 5.59] \text{ km/s}$, are summarized in Fig. 6. The minimum flight time t_f as a function of a_{\oplus} and V_{∞} is similar to that found for both Mercury and Venus. In particular, in this case for medium-high values of the characteristic acceleration ($a_{\oplus} > 1.5 \text{ mm/s}^2$) the flight time is nearly insensitive to a_{\oplus} . Also note that, for a given value of a_{\oplus} (that is, for a given value of sail performance) there exists a value of V_{∞} that minimizes the dimensionless flight time t_{on}/t_f . This condition corresponds to the optimal choice if one needs to minimize the likelihood of a propulsion system failure during the mission. The presence of a minimum value in the curves in Fig. 6(b) can be physically explained by analyzing the trajectories drawn in Fig. 7, corresponding to $a_{\oplus} = 1 \text{ mm/s}^2$. In a low-thrust transfer, as that obtainable with an electric sail of small-medium performance, the rendezvous trajectory ($V_{\infty} = 0$, see Fig. 7(a)) is usually characterized by two propelled phases, alternated with a coasting phase ($\tau = 0$). Such a typical

behavior for circular coplanar orbits was first pointed out by Lawden [25] and then studied in detail by Alfano and Thorne [29]. In essence, the first propelled phase serves to increase the semimajor axis of the osculating orbit, and to insert the spacecraft on the proper transfer trajectory. The semimajor axis increase involves, as a secondary effect, a parallel increase of the orbit eccentricity. The latter must be necessarily reduced to zero with a succeeding propelled phase because the target orbit is, by assumption, perfectly circular. This behavior is better understood with the aid of Fig. 8 that shows, as a function of time, the semimajor axis a and the eccentricity e of the osculating orbit for an Earth-Mars rendezvous trajectory with an electric sail having $a_{\oplus} = 1 \text{ mm/s}^2$.

The possible presence of an intermediate coasting phase is closely related to the actual direction of the primer vector, see Eq. (19). The length of the coasting phase, in terms of mission time fraction, is essentially dependent, for a rendezvous mission, on the value of a_{\oplus} . Usually, small values of a_{\oplus} correspond to short coasting phases.

If a final hyperbolic excess speed different from zero is allowed, the morphology of the optimal transfer trajectory varies. In fact, as V_{∞} is increased, the length of the final propelled phase decreases. At the same time the coasting phase length tends to increase substantially, while the first phase of the propelled flight experiences a minor variation. When V_{∞} reaches the value that minimizes the ratio t_{on}/t_f (see Fig. 6(b)), the final propelled phase disappears, as shown in Fig. 7(b). In the latter case the whole trajectory is constituted by two phases only: a first phase with accelerated flight ($\alpha > 0$) and a succeeding coasting phase up to the mission end. A further increase of V_{∞} , see Fig. 7(c), involves an increase of the propelled phase and a reduction of the coasting phase. This behavior is ultimately responsible of the appearance of the minima in the curve t_{on}/t_f as a function of V_{∞} , see Fig. 6(b). The optimal value of V_{∞} , which minimizes the ratio t_{on}/t_f , is shown in Fig. 9 as a function of $a_{\oplus} \in [0.5, 2] \text{ mm/s}^2$.

3.2 Mission Towards Outer Planets

The advantage of using an electric sail for flyby missions towards the outer planets (Jupiter, Saturn, Uranus, and Neptune) is confirmed by Figs 10–13. To obtain transfer trajectories with reasonable mission times, we confine our analysis to characteristic accelerations ranging in the interval $[1, 2] \text{ mm/s}^2$ and hyperbolic excess speeds $V_\infty \in [0.5, 1] \Delta V_H$. Using the data from Table 1, the above values correspond to flyby trajectories in which the final value of hyperbolic excess speed ranges between 7 km/s and 16 km/s.

When compared to the previous missions towards inner planets, the analysis of an Earth–Jupiter mission (see Fig. 10) with a two-dimensional approach provides rather accurate simulation results. This is due to the small values of orbit eccentricity ($e \cong 0.04839$) and inclination ($i \cong 1.3 \text{ deg}$). From Fig. 10(a), the flight times vary from about 2.15 years (for $V_\infty = 0.5 \Delta V_H$) down to 1.6 years (for $V_\infty = \Delta V_H$). Because in this case the total velocity variation for an Hohmann transfer is substantial ($\Delta V_H \simeq 14.43 \text{ km/s}$), it can be verified that further increases of V_∞ do not imply any significant improvement in mission performance in terms of flight time.

The relationship between t_f/t_H and $V_\infty/\Delta V_H$ can be approximated, with an error less than 10^{-3} , by the formula

$$\frac{t_f}{t_H} = b_1 \left(\frac{V_\infty}{\Delta V_H} \right)^{b_2} + b_3 \quad \text{with} \quad V_\infty \in [0.5, 1] \Delta V_H \quad (23)$$

where b_1 , b_2 , and b_3 are suitable interpolating coefficients, depending on the characteristic acceleration, and whose values are shown in Table 2.

The value of V_∞ remarkably affects the dimensionless thrusting time t_{on}/t_f . In fact assuming $a_\oplus = 1 \text{ mm/s}^2$, Fig. 10(b) shows that if one varies the hyperbolic excess speed from $V_\infty = 0.5 \Delta V_H$ to $V_\infty = \Delta V_H$, the thrusting time increases from 31.5% to 80% of the flight time. This

behavior is also shown in Fig. 14, which illustrates the control law and the optimal trajectory for two different values of the hyperbolic excess velocity.

As long as transfers towards Saturn, Uranus, and Neptune are concerned, Figs. 11–13 show similar trends for both the flight time and the dimensionless thrusting time. In particular, in all of the simulations the sailcraft reaches the target in less than a full revolution around the Sun.

3.3 Performance comparison

A simple analysis in terms of required velocity variations can be established by comparing a chemical propulsion based spacecraft and a hybrid configuration that combines a chemical thruster with an electric sail. To this end, assume that the spacecraft is initially placed on a circular parking orbit around the Earth with a height $h_c = 200$ km and that the capture orbit around the target planet is characterized by a pericenter height $h_p = 1\,000$ km. Consider a two-dimensional trajectory described through a patched conic approximation and a biimpulsive transfer. The first velocity variation is employed to leave the parking orbit, while the second ΔV is used to close the orbit around the target planet. For a transfer with a pure chemical propulsion system, the heliocentric transfer phase is obtained with a flight by inertia [30]. For an hybrid system, instead, the electric sail is exploited in the heliocentric phase to obtain the desired final value of V_∞ . Let ΔV_{esc} and ΔV_{cap} be, respectively, the first and second velocity variations due to the chemical thruster. One has [30]:

$$\Delta V_{\text{esc}} = \sqrt{\frac{2\mu_\oplus}{R_\oplus + h_c} + C_3} - \sqrt{\frac{\mu_\oplus}{R_\oplus + h_c}} \quad (24)$$

$$\Delta V_{\text{cap}} = \sqrt{\frac{2\mu}{R_p + h_p} + V_\infty^2} - \sqrt{\frac{2\mu}{R_p + h_p}} \quad (25)$$

where C_3 is the escape orbit characteristic energy [31], whereas R_p and μ are the target planet mean radius and gravitational parameter, respectively (R_\oplus and μ_\oplus refer to Earth). The required total variation of velocity, ΔV_{tot} , is the sum of ΔV_{esc} and ΔV_{cap} . Note that for an hybrid propulsion system $C_3 = 0$ in Eq. (24) because, by assumption, the electric sail follows an escape parabolic orbit. Assuming for the hybrid configuration $V_\infty = \Delta V_H/2$ (see Table 1) and $a_\oplus = 1 \text{ mm/s}^2$, the simulation results have been summarized in Table 3 and compared with the results corresponding to a biimpulsive Hohmann transfer. The table shows that the hybrid configuration guarantees a substantial reduction in the required total velocity variation with respect to the Hohmann transfer. In particular, the hybrid configuration is especially advantageous for transfers towards outer planets. For example, in a mission to Jupiter, the ΔV_{tot} saving is of 44%, with a shorter (around 6 months) flight time, while a mission to Neptune guarantees a ΔV_{tot} saving of 47% and a flight time decrease of 15 years. Note however that such a performance increase for an hybrid configuration (in particular, the ΔV_{tot} saving) does not imply a proportional increase of the corresponding payload mass fraction deliverable. To better discuss the latter point and obtain a first estimate of the payload mass fraction deliverable, we now introduce a simplified spacecraft mass breakdown model in which the spacecraft launch mass m_0 is obtained as the sum of three contributions: 1) the payload mass m_{pay} (which coincides with the spacecraft mass at the end of the capture phase), 2) the electric sail mass m_{sail} (comprising the structural mass necessary to join the payload with the sail), and 3) the propellant mass m_{prop} required by the chemical thrusters. Accordingly

$$m_0 = m_{\text{pay}} + m_{\text{sail}} + m_{\text{prop}} \quad (26)$$

For a transfer with a chemical propulsion system, instead, the launch mass m_0 is simply the sum of m_{pay} e di m_{prop} . Consider first a chemical propulsion based option (subscript C). From

the rocket equation, the payload mass fraction $\sigma_{\text{pay}} \triangleq m_{\text{pay}}/m_0$ is given by

$$\sigma_{\text{pay}_C} = \exp\left(-\frac{\Delta V_{\text{tot}_C}}{g_0 I_{sp}}\right) \quad (27)$$

where g_0 is the Earth's standard gravitational acceleration and I_{sp} is the chemical thruster specific impulse. Note that σ_{pay_C} is univocally defined as a function of the propulsive characteristics (I_{sp}) and of the mission strategy (in terms of ΔV_{tot_C}). For example, in an Earth-Jupiter Hohmann transfer (see Table 3) where $I_{sp} = 350$ s, the payload mass fraction is $\sigma_{\text{pay}} = 0.147$.

As far as the hybrid solution is concerned (subscript E), assuming that the sail is jettisoned before entering into the sphere of influence of the target planet, one obtains:

$$\sigma_{\text{pay}_E} = \left[\exp\left(-\frac{\Delta V_{\text{esc}_E}}{g_0 I_{sp}}\right) - \sigma_{\text{sail}} \right] \exp\left(-\frac{\Delta V_{\text{cap}_E}}{g_0 I_{sp}}\right) \quad (28)$$

where $\sigma_{\text{sail}} \triangleq m_{\text{sail}}/m_0$ is the sailcraft mass fraction. Taking into account the data summarized in Table 3, Eq. (28) states that σ_{pay_E} is an implicit function of a_{\oplus} and t_f through ΔV_{cap_E} , see Eqs. (23) and (25).

For the same values of launch mass and specific impulse, an hybrid solution requires a payload mass greater than a conventional (chemical) configuration provided that $\sigma_{\text{pay}_E} > \sigma_{\text{pay}_C}$. Note that there exists a critical value of sailcraft mass fraction, referred to as σ_{sail}^* , such that the two solutions (chemical and hybrid) provide the same payload mass fraction deliverable, that is, $\sigma_{\text{pay}_E} = \sigma_{\text{pay}_C}$. Accordingly, with the aid of Eqs. (27)–(28), the condition $\sigma_{\text{pay}_E} > \sigma_{\text{pay}_C}$ can be translated into the following inequality involving σ_{sail} :

$$\sigma_{\text{sail}} < \sigma_{\text{sail}}^* \triangleq \exp\left(-\frac{\Delta V_{\text{esc}_E}}{g_0 I_{sp}}\right) - \exp\left(\frac{\Delta V_{\text{cap}_E} - \Delta V_{\text{tot}_C}}{g_0 I_{sp}}\right) \quad (29)$$

which implicitly relates σ_{sail}^* with the characteristic acceleration a_{\oplus} and the minimum flight time t_f . Equation (29) can be effectively represented in graphical form once that the target

planet is given. For example, taking into account the data of Tables 2-3, Fig. 15 shows the contours of σ_{sail}^* as a function a_{\oplus} and t_f for an Earth-Jupiter transfer. Assuming a flight time $t_f = 2$ years and a characteristic acceleration $a_{\oplus} = 1 \text{ mm/s}^2$, the hybrid option provides a payload mass fraction deliverable greater than that corresponding to a chemical case provided that the sail mass fraction is less than 0.216.

4 Conclusions

Optimal interplanetary rendezvous missions combining electric sail and high-thrust propulsion systems have been studied in an optimal framework. Missions towards both the inner and the outer planets of the Solar System have been simulated. Each transfer mission has been investigated in a parametric way for different values of characteristic acceleration and hyperbolic excess speed with respect to the target planet. The simulations show that the combined use of an electric sail with a chemical thruster is capable of reducing the propellant amount required to accomplish a given mission transfer. The reduction of propellant mass can be translated into a corresponding increase of payload mass fraction deliverable provided that the electric sail mass is less than a critical value. Such a value is a function of both the flight time and the sail characteristic acceleration and can be estimated with the aid of a suitable mass breakdown model. The obtained results confirm the viability and potentiality of such a hybrid configuration.

References

- [1] R. L. McNutt, Solar system exploration: A vision for the next hundred years, in: 55th International Astronautical Congress of the International Astronautical Federation, the International Academy of Astronautics, and the International Institute of Space Law, Paper IAC-04-IAA.3.8.1.02,

Vancouver, Canada, 2004.

- [2] R. S. Saunders, Nasa's solar system exploration program, in: AIAA Space 2000 Conference and Exposition, Paper AIAA-2000-5324, Long Beach, CA, 2000.
- [3] J. R. Brophy, Advanced ion propulsion systems for affordable deep-space missions, *Acta Astronautica* 52 (2–6) (2003) 309–316.
- [4] J. R. Brophy, M. Noca, Electric propulsion for solar system exploration, *Journal of Propulsion and Power* 14 (5) (1998) 700–707.
- [5] R. Gershman, C. Seybold, Propulsion trades for space science missions, *Acta Astronautica* 45 (4–9) (1999) 541–548.
- [6] R. Gershman, R. A. Wallace, Technology needs of future planetary missions, *Acta Astronautica* 45 (4–9) (1999) 329–335.
- [7] J. A. Kechichian, Optimal low-thrust transfer using variable bounded thrust, *Acta Astronautica* 36 (7) (1995) 357–365.
- [8] G. Mengali, A. A. Quarta, Optimal trade studies of interplanetary electric propulsion missions, *Acta Astronautica* 62 (12) (2008) 657–667.
- [9] G. Mengali, A. A. Quarta, Optimal heliostationary missions of high-performance sailcraft, *Acta Astronautica* 60 (8–9) (2007) 676–683.
- [10] A. A. Quarta, G. Mengali, Solar sail missions to mercury with venus gravity assist, *Acta Astronautica* 65 (3–4) (2009) 495–506.
- [11] G. Mengali, A. A. Quarta, Optimal control laws for axially symmetric solar sails, *Journal of Spacecraft and Rockets* 42 (6) (2005) 1130–1133.
- [12] G. Mengali, A. A. Quarta, Solar-sail-based stopover cyclers for cargo transportation missions, *Journal of Spacecraft and Rockets* 44 (4) (2007) 822–830.
- [13] P. Janhunen, A. Sandroos, Simulation study of solar wind push on a charged wire: Basis of solar wind electric sail propulsion, *Annales Geophysicae* 25 (3) (2007) 755–767.

- [14] P. Janhunen, On the feasibility of a negative polarity electric sail, *Annales Geophysicae* 27 (4) (2009) 1439–1447.
- [15] P. Janhunen, Electric sail for spacecraft propulsion, *Journal of Propulsion and Power* 20 (4) (2004) 763–764.
- [16] G. Mengali, A. A. Quarta, P. Janhunen, Electric sail performance analysis, *Journal of Spacecraft and Rockets* 45 (1) (2008) 122–129.
- [17] G. Mengali, A. A. Quarta, P. Janhunen, Considerations of electric sailcraft trajectory design, *Journal of the British Interplanetary Society* 61 (2008) 326–329.
- [18] P. Janhunen, G. Mengali, A. A. Quarta, Electric sail propulsion modeling and mission analysis, 30th International Electric Propulsion Conference, Florence, Italy, 2007, paper IEPC-2007-352.
- [19] P. Janhunen, The electrical sail - a new propulsion method which may enable fast missions to the outer solar system, *Journal of the British Interplanetary Society* 61 (2008) 322–325.
- [20] G. Mengali, A. A. Quarta, Non-keplerian orbits for electric sails, *Celestial Mechanics and Dynamical Astronomy* in press, doi: 10.1007/s10569-009-9200-y.
- [21] P. Janhunen, Status report of the electric sail - a revolutionary near-term propulsion technique in the solar system, Sixth IAA Symposium on Realistic Near-Term Advanced Scientific Space Missions, Aosta, Italy, 2009.
- [22] M. Leipold, M. Götz, Hybrid photonic/electric propulsion, Tech. Rep. SOL4-TR-KTH-0001, Kayser-Threde GmbH, Munich, Germany, ESA contract No. 15334/01/NL/PA (January 2002).
- [23] G. Mengali, A. A. Quarta, Trajectory design with hybrid low-thrust propulsion system, *Journal of Guidance, Control, and Dynamics* 30 (2) (2007) 419–426.
- [24] A. E. Bryson, Y. C. Ho, *Applied Optimal Control*, Hemisphere Publishing Corporation, New York, NY, 1975, Ch. 2, pp. 71–89.
- [25] D. F. Lawden, *Optimal Trajectories for Space Navigation*, Butterworths, London, 1963, pp. 54–68.

- [26] R. S. Nah, S. R. Vadali, E. Braden, Fuel-optimal, low-thrust, three-dimensional earth-mars trajectories, *Journal of Guidance, Control, and Dynamics* 24 (6) (2001) 1100–1107.
- [27] G. Mengali, A. A. Quarta, Fuel-optimal, power-limited rendezvous with variable thruster efficiency, *Journal of Guidance, Control, and Dynamics* 28 (6) (2005) 1194–1199.
- [28] R. F. Stengel, *Optimal Control and Estimation*, Dover Publications, Mineola, NY, 1994, pp. 222–254.
- [29] S. Alfano, J. D. Thorne, Circle-to-Circle Constant-Thrust Orbit Raising, *Journal of the Astronautical Sciences* 42 (1) (1994) 35–45.
- [30] C. D. Brown, *Spacecraft Mission Design*, AIAA Education Series, American Institute of Aeronautics and Astronautics, 370 L’Enfant Promenade, SW, Washinton DC, 1992, Ch. 6, pp. 95–130.
- [31] V. A. Chobotov, *Orbital Mechanics*, 2nd Edition, AIAA Education Series, American Institute of Aeronautics and Astronautics, 370 L’Enfant Promenade, SW, Washinton DC, 1996, Ch. 12, p. 278.

List of Tables

1	Earth-Planet Hohmann transfer performance.	22
2	Fitting coefficients (see Eq. (23)).	23
3	Biimpulsive interplanetary transfer ΔV budget: chemical vs hybrid performance.	24

Planet	r_p [AU]	ΔV_H [km/s]	t_H [years]
Mercury	0.387	17.144	0.289
Venus	0.723	5.202	0.399
Mars	1.524	5.593	0.708
Jupiter	5.203	14.436	2.731
Saturn	9.537	15.731	6.046
Uranus	19.191	15.940	16.039
Neptune	30.069	15.707	30.613

Table 1
Earth-Planet Hohmann transfer performance.

Planet	a_{\oplus} [mm/s ²]	b_1	b_2	b_3
Jupiter	1.0	0.1288	-1.3980	0.4569
	1.5	0.2929	-0.8913	0.2138
	2.0	0.3217	-0.8588	0.1598
Saturn	1.0	0.1404	-1.284	0.3328
	1.5	0.3172	-0.7988	0.0945
	2.0	0.344	-0.7682	0.0519
Uranus	1.0	0.196	-0.9835	0.1541
	1.5	0.3133	-0.7379	0.0042
	2.0	0.3273	-0.7221	-0.0172
Neptune	1.0	0.2129	-0.8835	0.0746
	1.5	0.2911	-0.7249	-0.0230
	2.0	0.2996	-0.7141	-0.0357

Table 2
Fitting coefficients (see Eq. (23)).

Planet	Hohmann transfer				Hybrid option				
	ΔV_{esc} [km/s]	ΔV_{cap} [km/s]	ΔV_{tot} [km/s]	t_H [years]	ΔV_{esc} [km/s]	ΔV_{cap} [km/s]	ΔV_{tot} [km/s]	V_{∞} [km/s]	t_f [years]
Mercury	5.554	6.677	12.232	0.289	3.224	5.710	8.934	8.572	0.598
Venus	3.503	0.374	3.878	0.399	3.224	0.346	3.570	2.601	0.520
Mars	3.611	0.733	4.344	0.708	3.224	0.811	4.035	2.796	0.631
Jupiter	6.305	0.266	6.571	2.731	3.224	0.434	3.658	7.218	2.155
Saturn	7.284	0.411	7.695	6.046	3.224	0.854	4.078	7.865	4.001
Uranus	7.978	0.511	8.489	16.039	3.224	1.463	4.688	7.970	8.653
Neptune	8.247	0.353	8.600	30.613	3.224	1.298	4.523	7.853	14.127

Table 3
Biimpulsive interplanetary transfer ΔV budget: chemical vs hybrid performance.

List of Figures

1	Reference frame and electric sail cone angle.	26
2	Optimal cone angle.	27
3	Optimal thrust cone angle α as a function of primer vector cone angle α_λ ($\alpha_{\max} = 35$ deg).	28
4	Earth-Mercury minimum-time missions performance as a function of a_\oplus and V_∞ .	29
5	Earth-Venus minimum-time missions performance as a function of a_\oplus and V_∞ .	30
6	Earth-Mars minimum-time missions performance as a function of a_\oplus and V_∞ .	31
7	Earth-Mars optimal trajectory and control angle time history ($a_\oplus = 1$ mm/s ²).	32
8	Semimajor axis end eccentricity of osculating orbit for an Earth-Mars rendezvous trajectory ($a_\oplus = 1$ mm/s ²).	33
9	Optimal Earth-Mars performance (minimum flight time t_f with minimum thruster operating time t_{on}).	34
10	Earth-Jupiter minimum-time missions performance as a function of a_\oplus and V_∞ .	35
11	Earth-Saturn minimum-time missions performance as a function of a_\oplus and V_∞ .	36
12	Earth-Uranus minimum-time missions performance as a function of a_\oplus and V_∞ .	37
13	Earth-Neptune minimum-time missions performance as a function of a_\oplus and V_∞ .	38
14	Earth-Jupiter optimal trajectory and control angle time history ($a_\oplus = 1$ mm/s ²).	39
15	Electric sail critical mass fraction σ_{sail}^* [see Eq. (29)] for an Earth-Jupiter transfer with $I_{sp} = 350$ s.	40

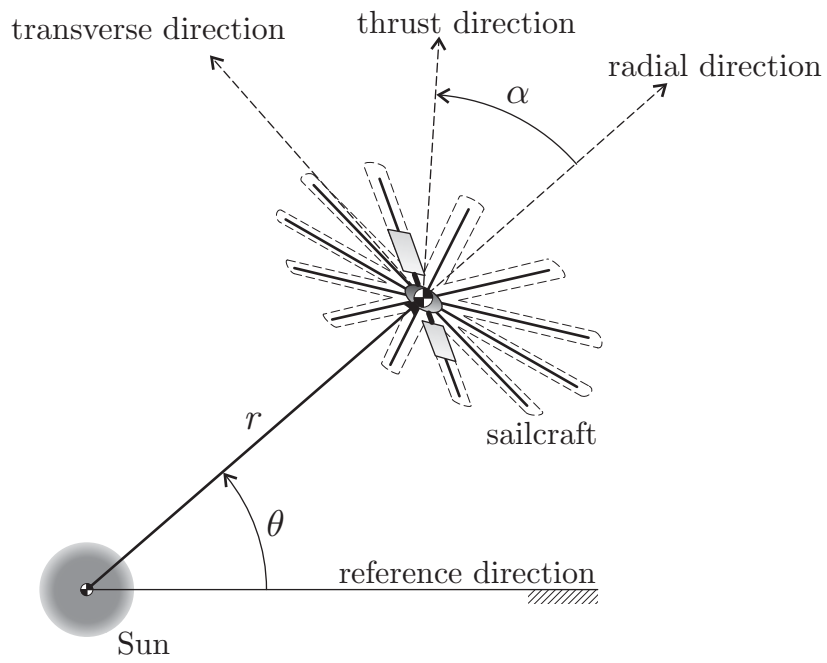


Figure 1. Reference frame and electric sail cone angle.

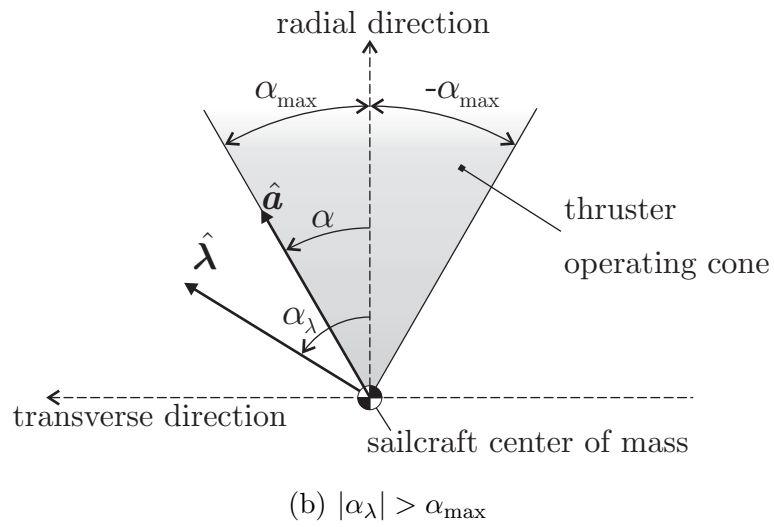
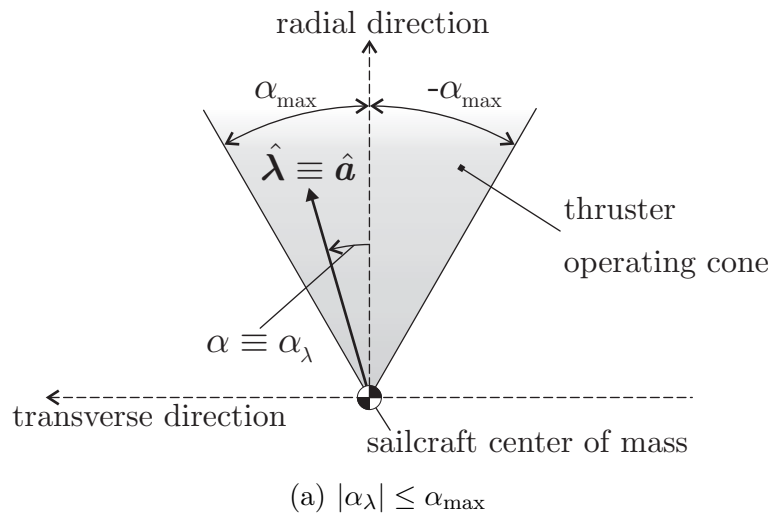


Figure 2. Optimal cone angle.

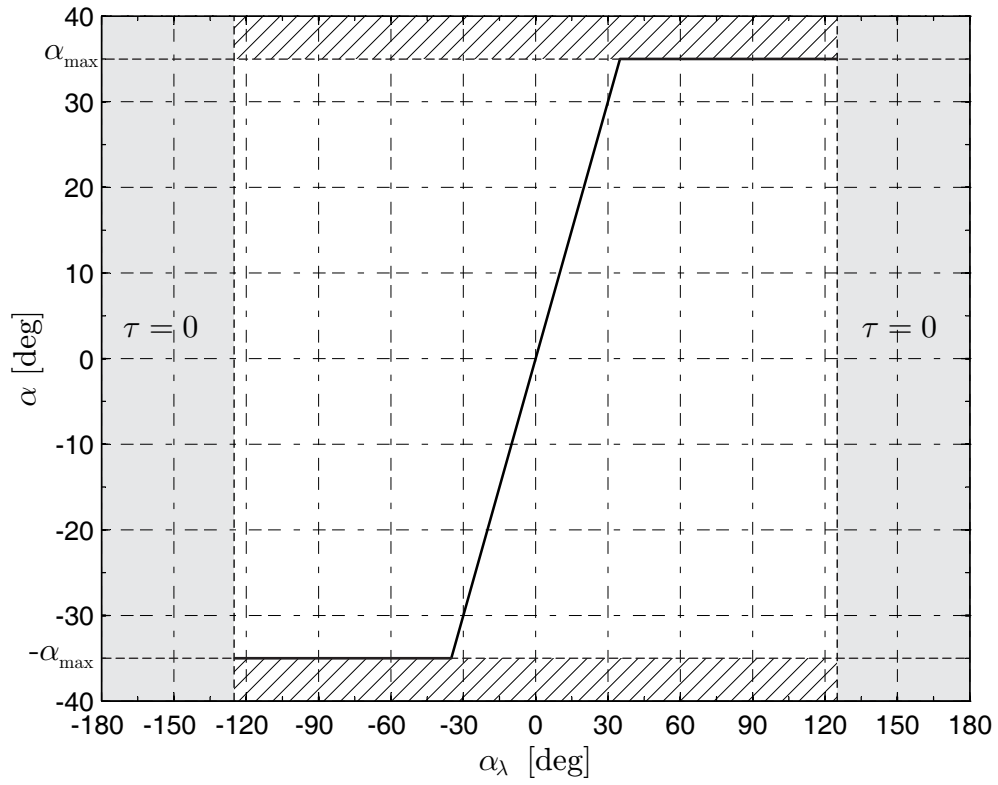
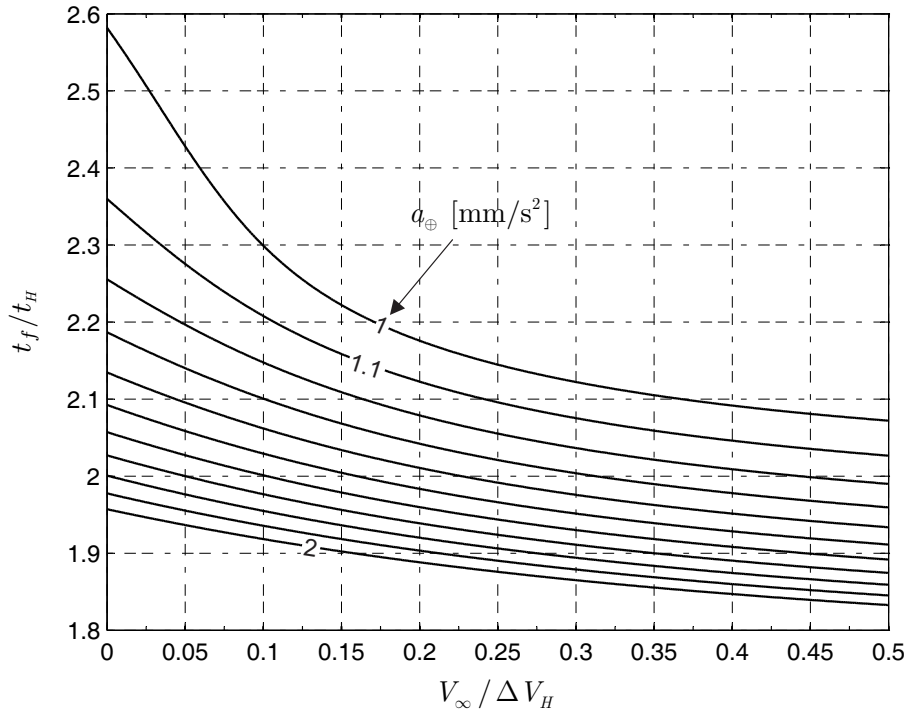
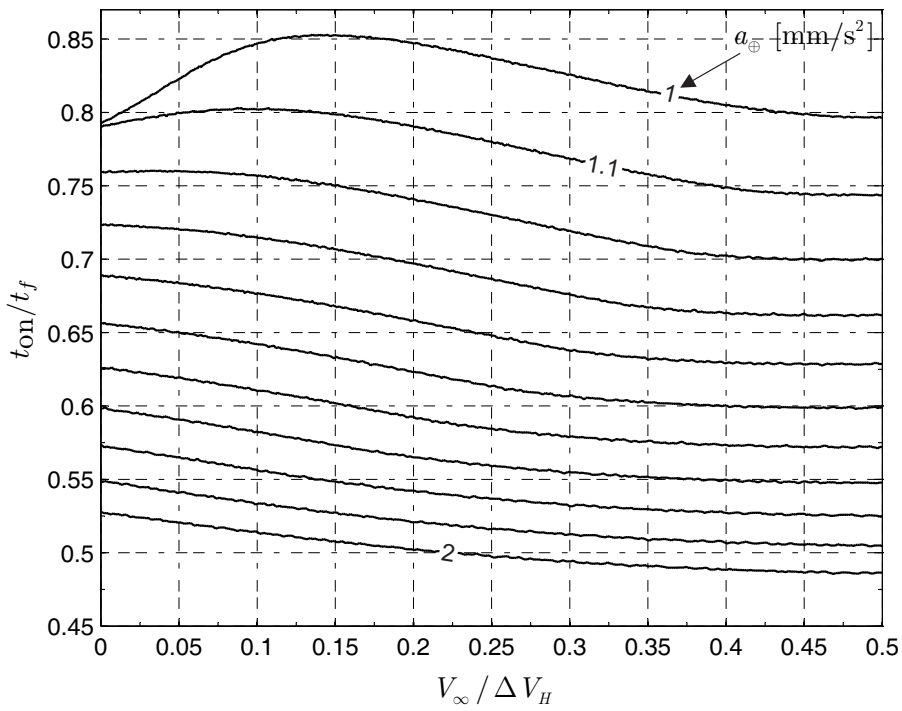


Figure 3. Optimal thrust cone angle α as a function of primer vector cone angle α_λ ($\alpha_{\max} = 35$ deg).

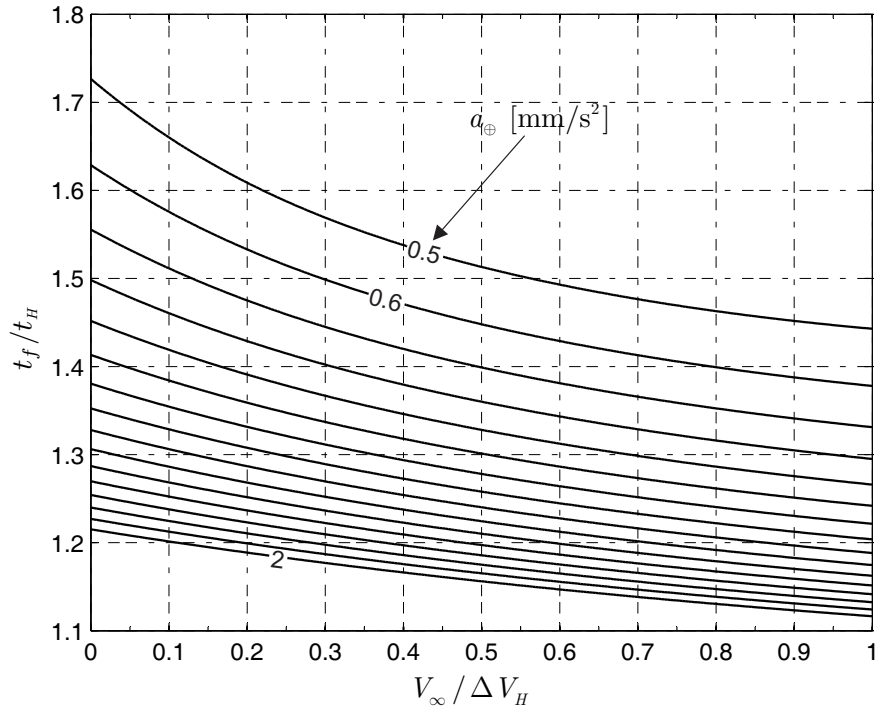


(a) Dimensionless minimum flight time

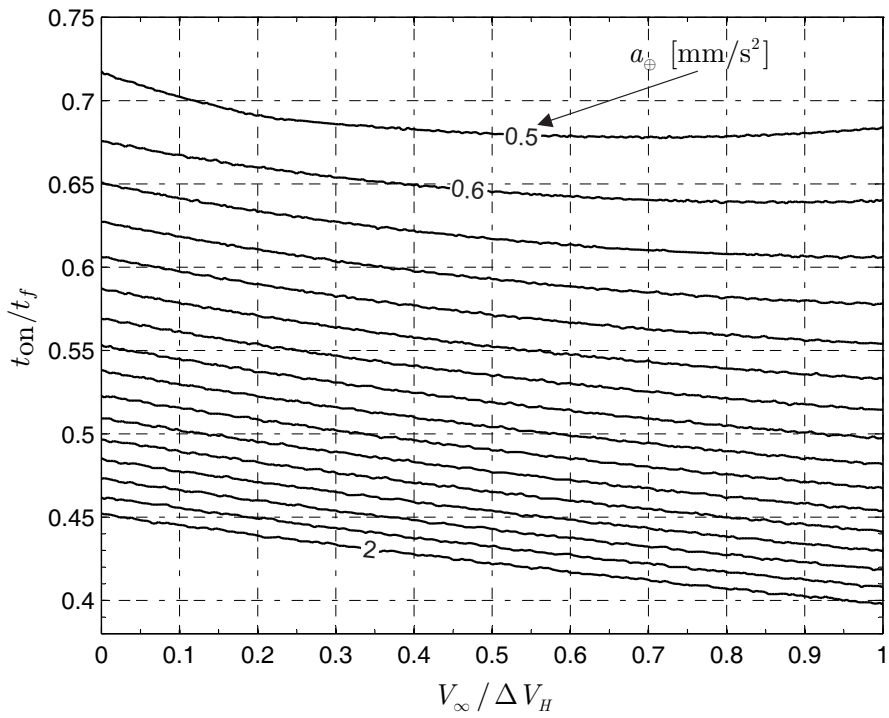


(b) Dimensionless thrusting time.

Figure 4. Earth-Mercury minimum-time missions performance as a function of a_\oplus and V_∞ .

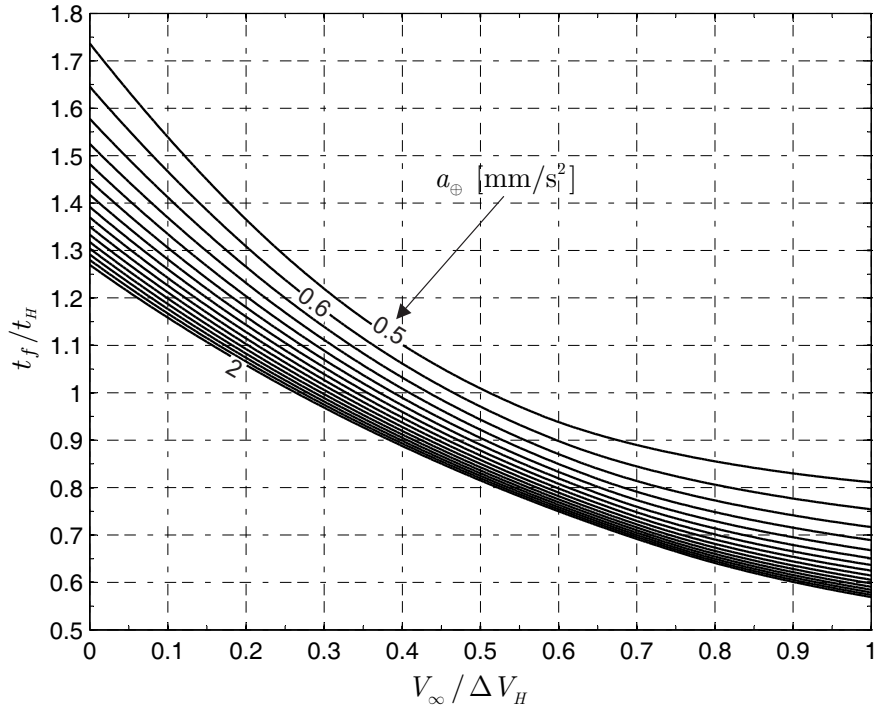


(a) Dimensionless minimum flight time

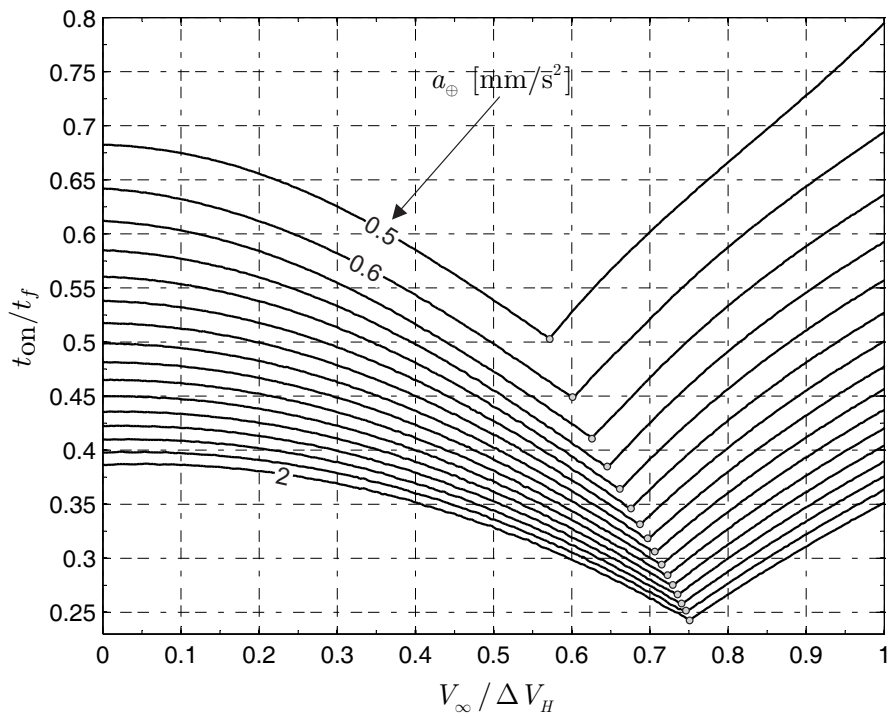


(b) Dimensionless thrusting time.

Figure 5. Earth-Venus minimum-time missions performance as a function of a_\oplus and V_∞ .

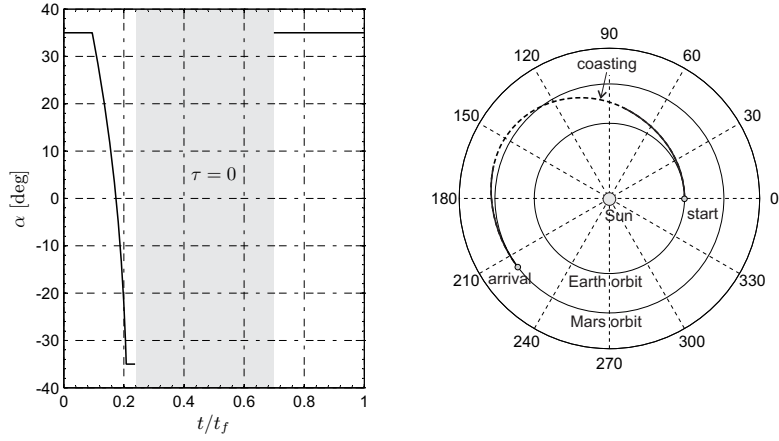


(a) Dimensionless minimum flight time

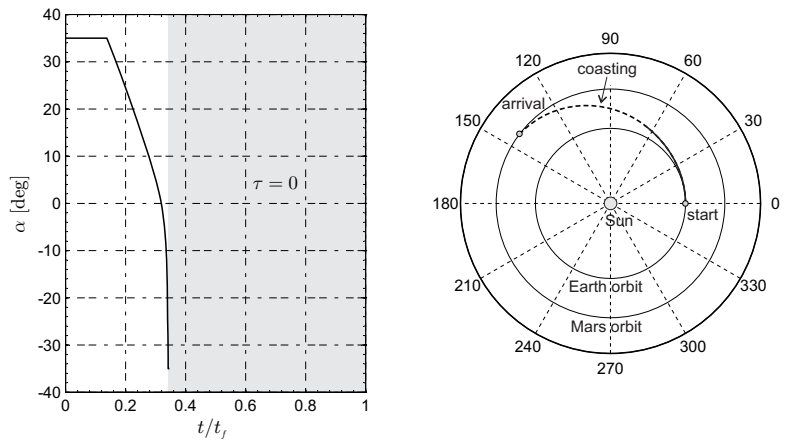


(b) Dimensionless thrusting time.

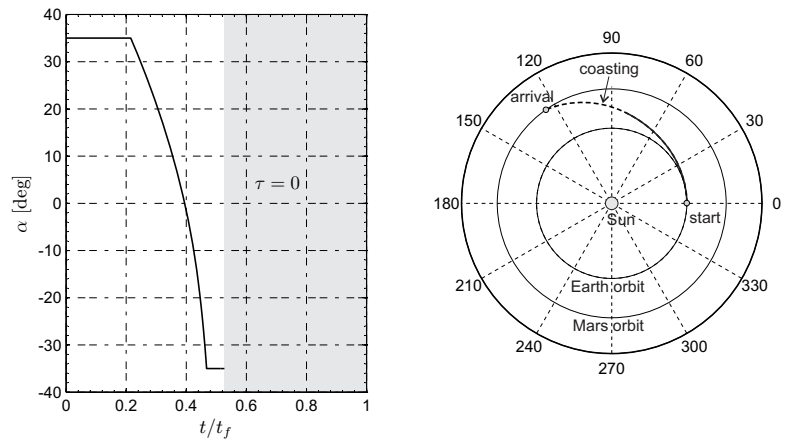
Figure 6. Earth-Mars minimum-time missions performance as a function of a_\oplus and V_∞ .



(a) $V_\infty = 0$ (rendezvous mission)



(b) $V_\infty = 0.676 \Delta V_H \simeq 3.78$ km/s (minimum thrusting time)



(c) $V_\infty = \Delta V_H \simeq 5.59$ km/s

Figure 7. Earth-Mars optimal trajectory and control angle time history ($a_\oplus = 1$ mm/s²).

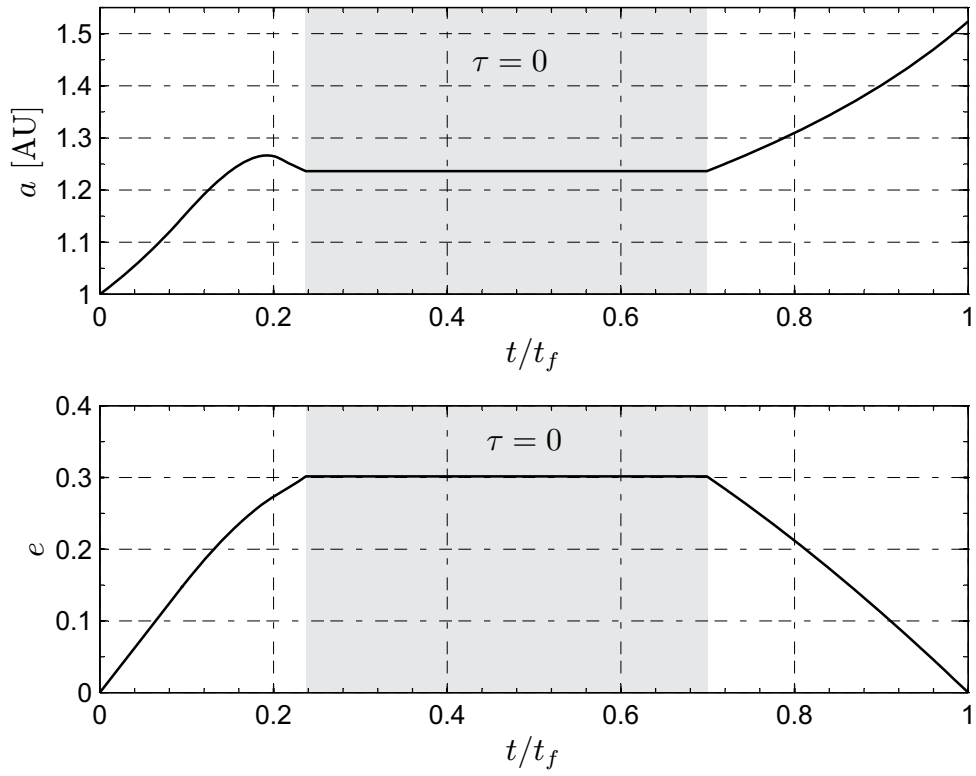


Figure 8. Semimajor axis and eccentricity of osculating orbit for an Earth-Mars rendezvous trajectory ($a_{\oplus} = 1 \text{ mm/s}^2$).

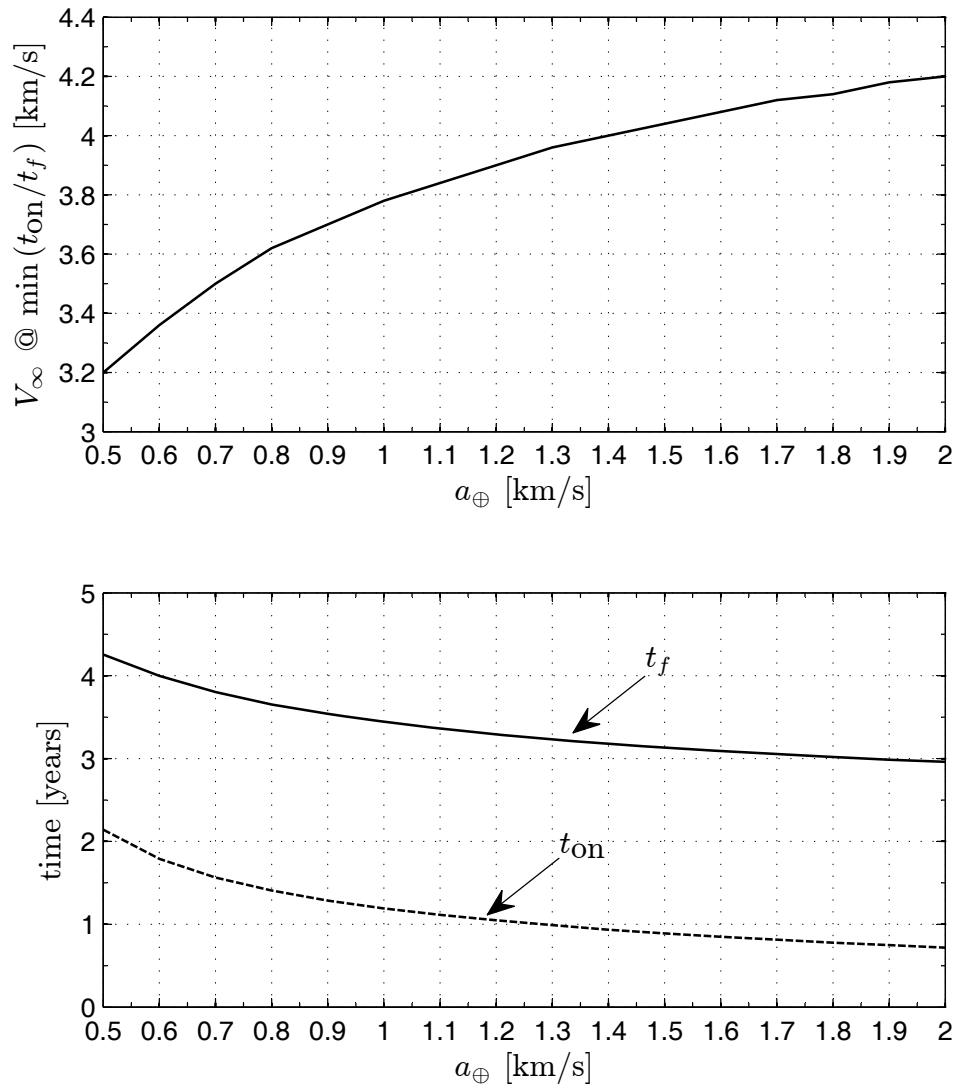
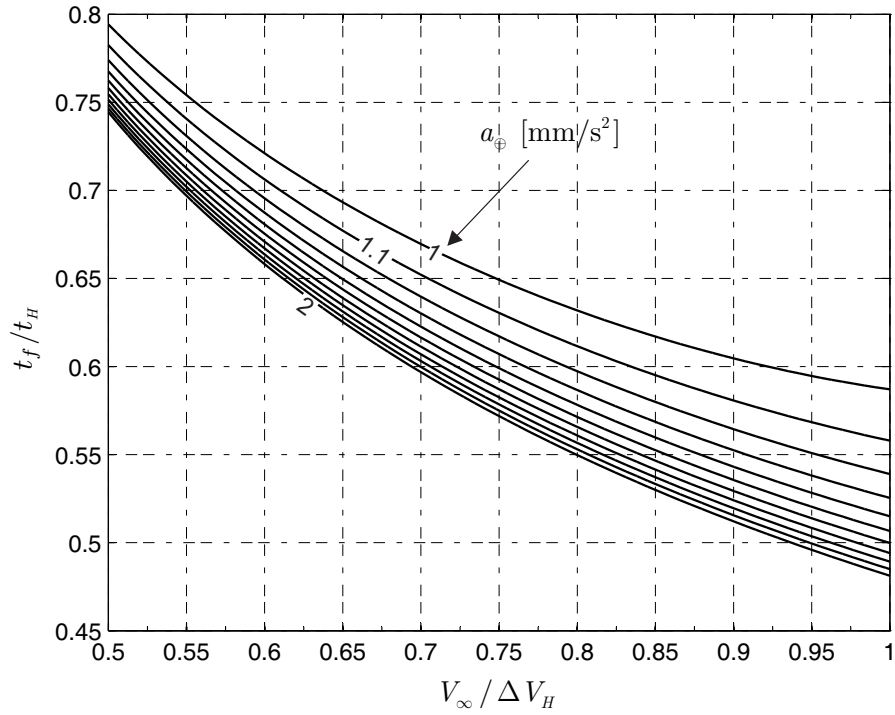
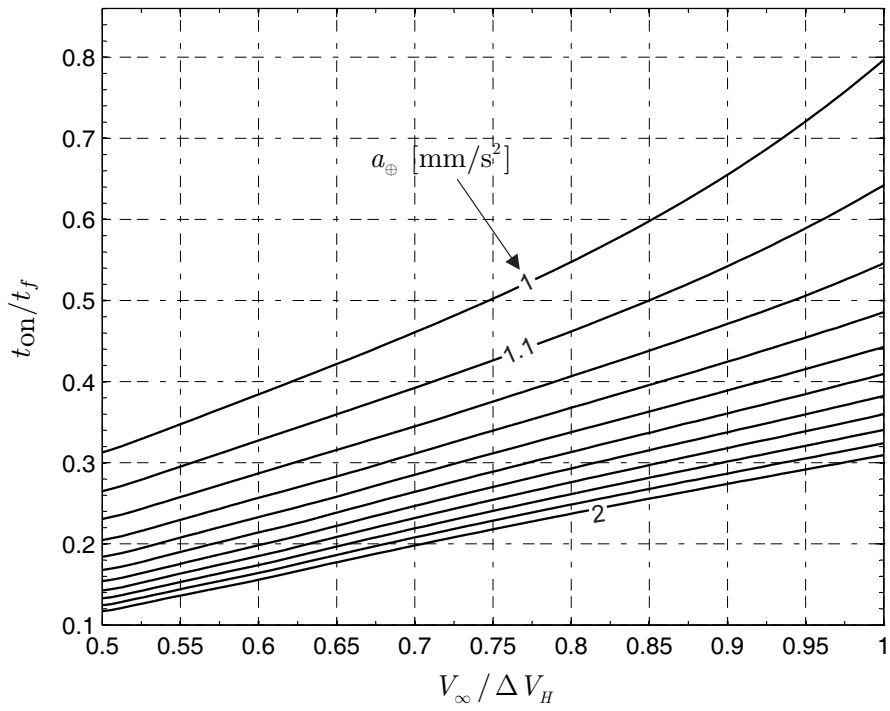


Figure 9. Optimal Earth-Mars performance (minimum flight time t_f with minimum thruster operating time t_{on}).

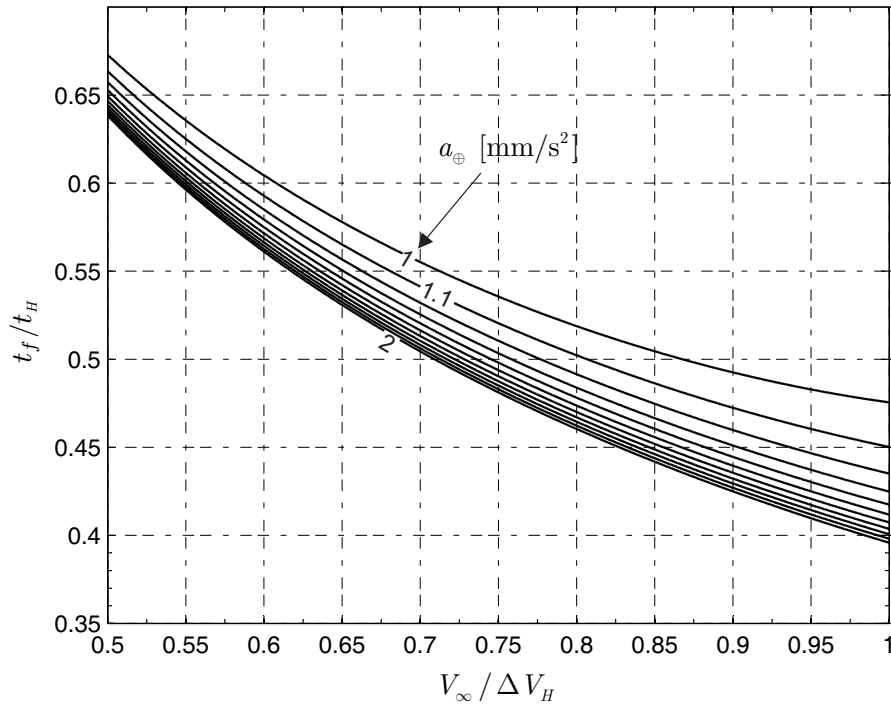


(a) Dimensionless minimum flight time

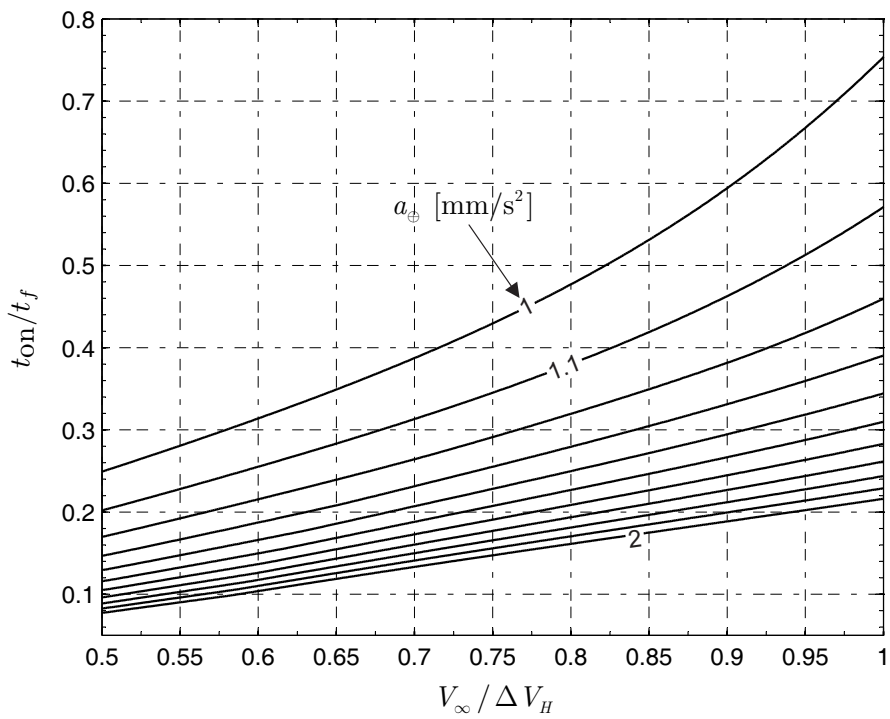


(b) Dimensionless thrusting time.

Figure 10. Earth-Jupiter minimum-time missions performance as a function of a_\oplus and V_∞ .

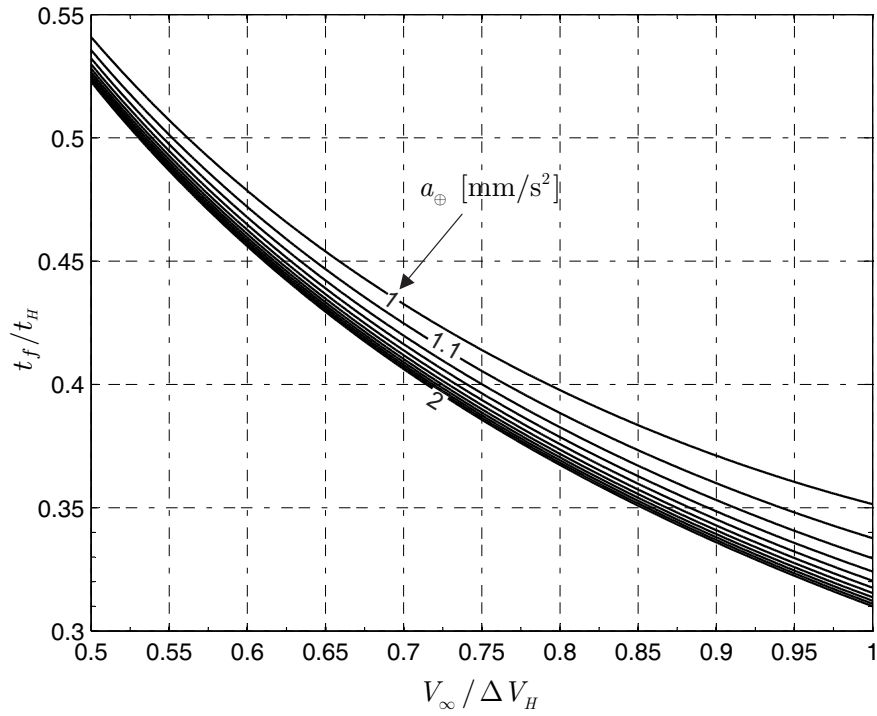


(a) Dimensionless minimum flight time

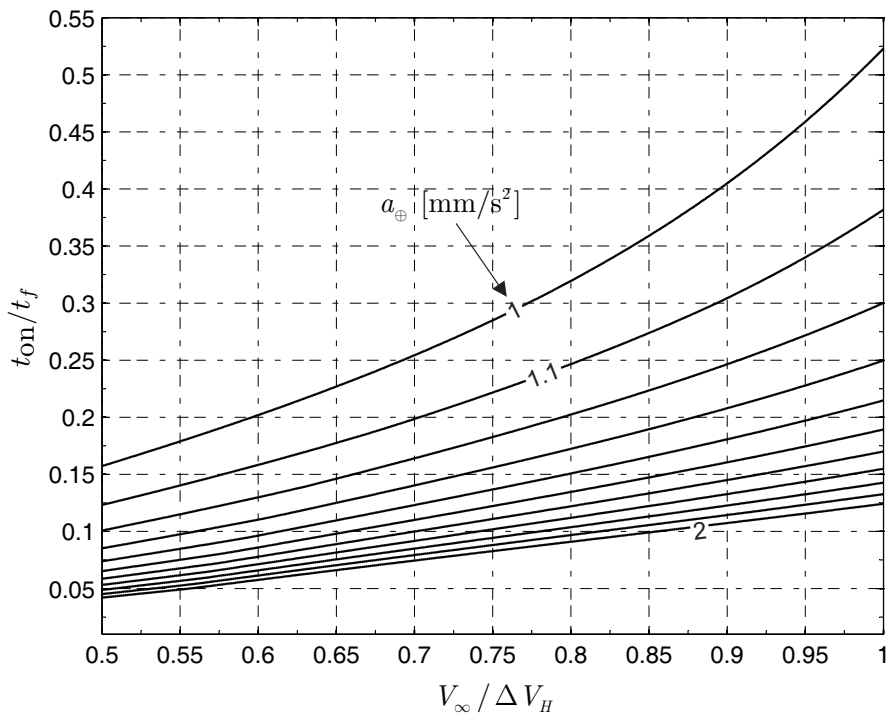


(b) Dimensionless thrusting time.

Figure 11. Earth-Saturn minimum-time missions performance as a function of a_\oplus and V_∞ .

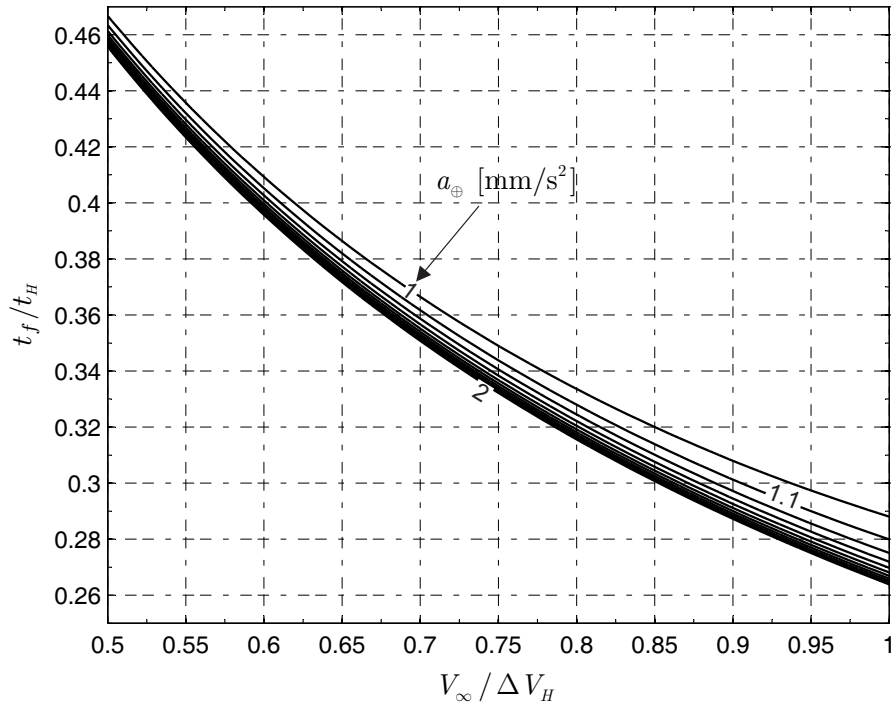


(a) Dimensionless minimum flight time

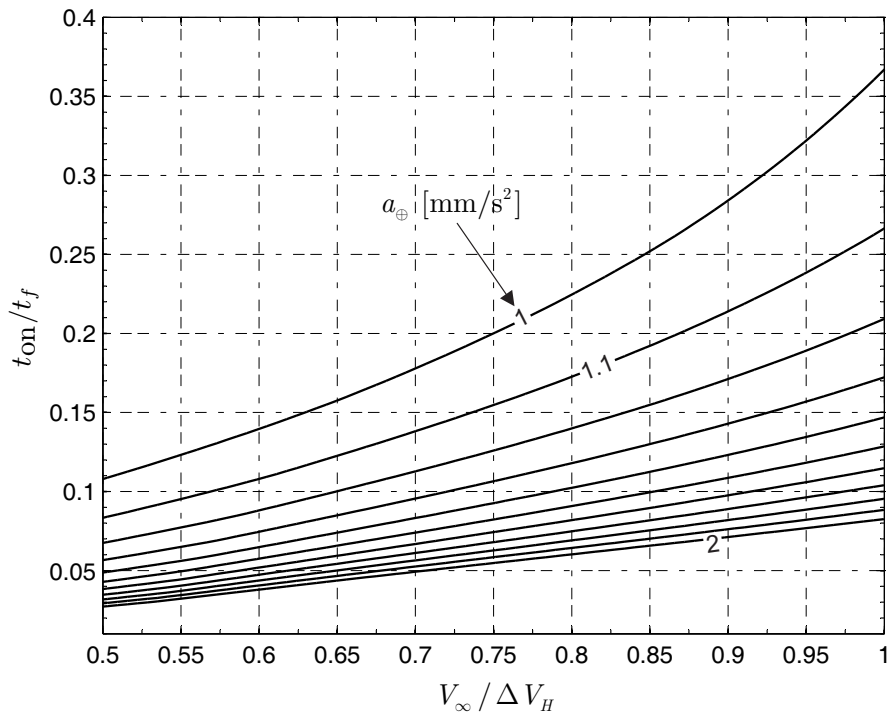


(b) Dimensionless thrusting time.

Figure 12. Earth-Uranus minimum-time missions performance as a function of a_\oplus and V_∞ .

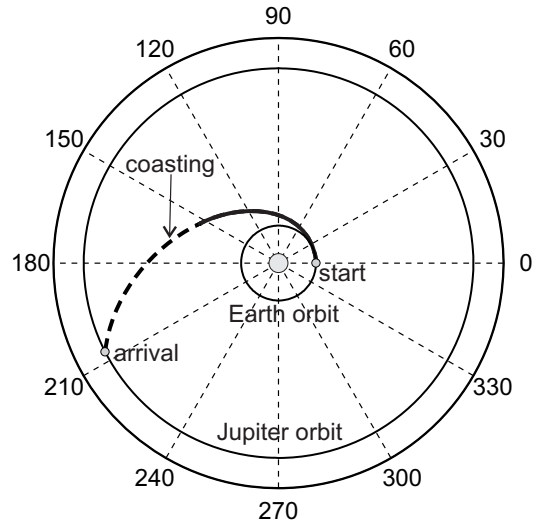
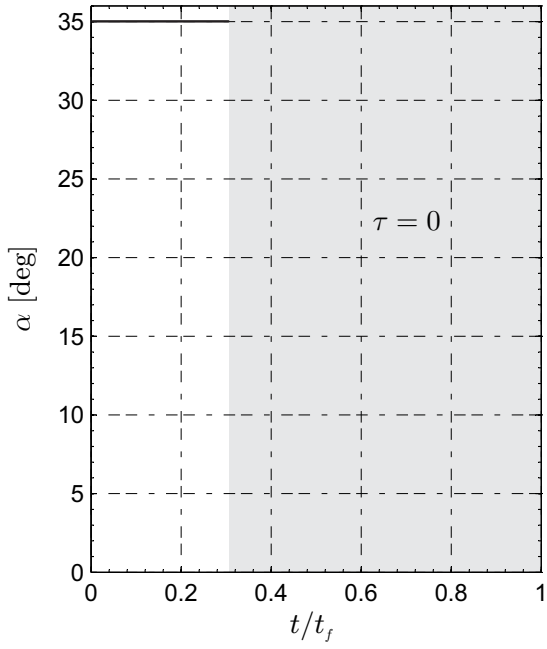


(a) Dimensionless minimum flight time

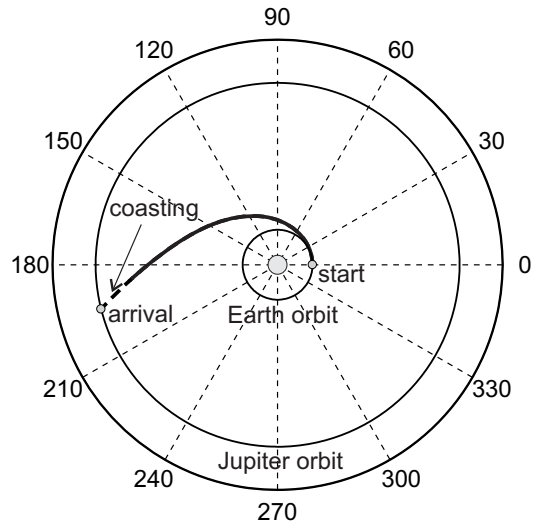
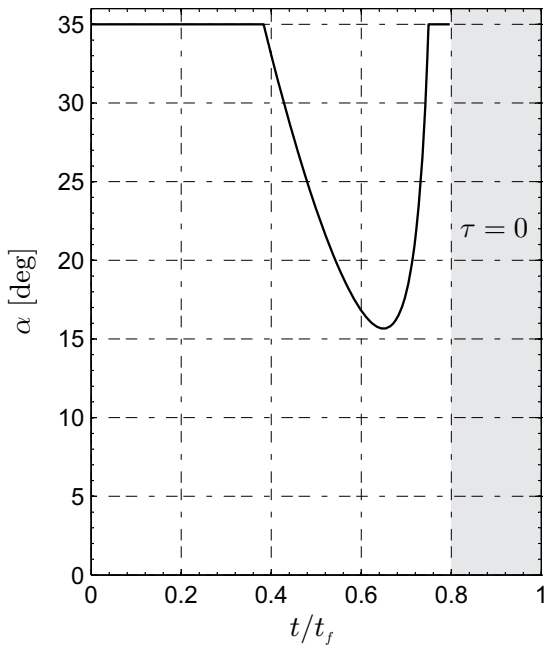


(b) Dimensionless thrusting time.

Figure 13. Earth-Neptune minimum-time missions performance as a function of a_\oplus and V_∞ .



(a) $V_\infty = 0.5 \Delta V_H \simeq 7.22 \text{ km/s}$



(b) $V_\infty = \Delta V_H \simeq 14.43 \text{ km/s}$

Figure 14. Earth-Jupiter optimal trajectory and control angle time history ($a_\oplus = 1 \text{ mm/s}^2$).

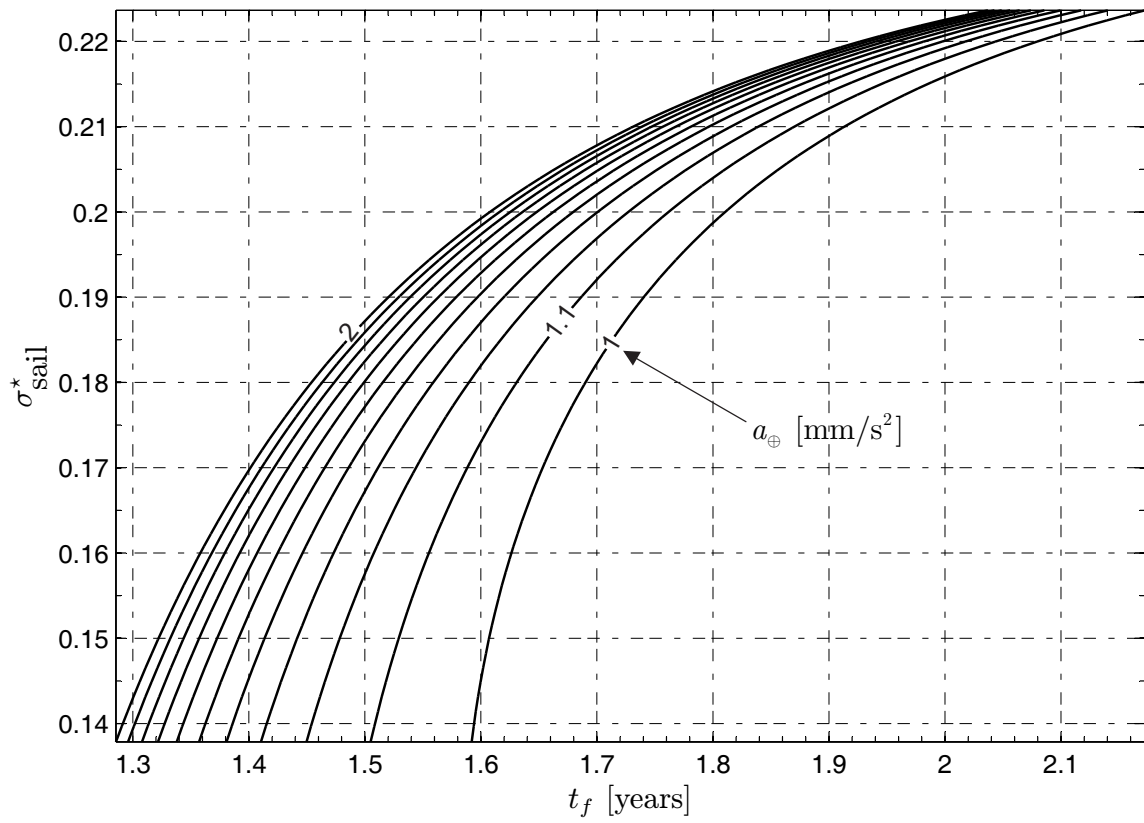


Figure 15. Electric sail critical mass fraction σ_{sail}^* [see Eq. (29)] for an Earth-Jupiter transfer with $I_{sp} = 350$ s.